CHAPTER IV

EXPERIMENTAL PROCEDURE

The experimental procedure in the fabrication of CIGS thin film solar cells involves several deposition techniques such as evaporation, sputtering and chemical bath deposition. A brief description of the deposition technique for each layer to complete the solar cells will be outlined. Particularly the emphasis is placed on the growth recipes of both CURO and CUPRO processes associating with a general calculation of temperature profile of these processes. In addition, the control process techniques using the *in situ* monitoring signals will be described. In order to understand the possible relationships between the CIGS film quality and the cell performance, it is necessary to investigate both the material characteristics and the cell performance. Therefore, the characterization techniques for structural, morphology and chemical composition of CIGS thin film will also be described.

4.1 Fabrication of CIGS Thin Film Solar Cells

The solar cell structure of Al(Ni)-grid/ZnO(Al)/CdS/CIGS/Mo on soda-lime glass (SLG) substrate is shown in Fig. 4.1. The fabrication process for CIGS thin film solar cells as shown in Fig. 4.2 can be described as the following.

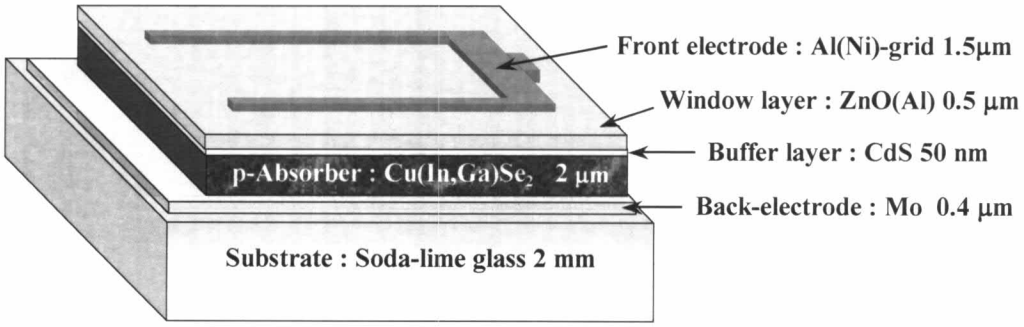

Figure 4.1: Schematic diagram (not to scale) of the CIGS thin film solar cell structure.

The SLG substrates were washed with detergent (e.g. liquid soap), rinsed in de-ionized water, then sequentially washed in an heating ultrasonic bath of diluted detergent and de-ionized water, and finally blown with nitrogen gas. This cleaning procedure has been shown to be suitable for a non-acid cleaning of the glass substrates.

The cleaned SLG substrates were coated with about 0.4 μm thick of molybdenum film by DC-magnetron sputtering. The standard deposition condition for good Mo back-electrode (e.g. low resistivity and good adhesion) was carried out using one deposition period of 10 min at the argon pressure of about $5x10^{-3}$ mbar and the sputtered current of 1 A.

The CIGS absorber layer was grown on the Mo/SLG substrate (2 mm in thickness and 5x6 cm^2 in area) by the multi-source co-evaporation technique. The four Knudsen-type sources were independently controlled by the programmable PID temperature controllers to emit appropriate fluxes of Cu, In, Ga and Se. The graphite heater temperature (T_{gh}) was controlled and kept constant by regulating the output power (OP) of the controller. The thermal radiation from the front surface of the substrate was monitored by the

pyrometer. During the deposition process (typically 1 hr), the substrate temperature (T_{sub}), the graphite heater temperature (T_{gh}), the heating output power (OP) and the temperature of the CIGS surface (T_{pyro}) were monitored simultaneously. By observing the variation of T_{pyro}, T_{sub} and OP, the desired Cu-deficient composition (end point detection: EPD) of the film can be obtained.

Typically, the CIGS films with the thickness ≈ 1.8-2.0 μm, ratios of [Ga]/([In]+[Ga]) ≈ 0.1-0.3, ratios of [Cu]/([In]+[Ga]) in the first stage ≈ 1.2-1.5 and final ratio of [Cu]/([In]+[Ga]) ≈ 0.9 (at the end of the process) were grown. The details of the growth recipes of both typical two-stage and modified two-stage were described in the latter parts.

Cadmium sulfide (CdS) buffer layer (thickness ≈ 50 nm) was deposited on the CIGS/Mo/SLG using chemical bath deposition (CBD) technique. Stock solution of specific quantities (mole/volume) of cadmium sulfate ($CdSO_4$ with 0.004 mol/50cc), thiourea ($SC(NH_2)_2$ with 0.06 mol/100cc) and ammonia solution (NH_3 with 4 mol/50cc) prepared at room temperature were used in our standard recipe for CBD-CdS technique. The CIGS/Mo/SLG sample was immediately immersed in the mixture of the stock solutions which was placed in the water bath kept at constant temperature 60°C. During the deposition time of about 10 minutes, the sample was shaken every minute. Immediately after the deposition, the sample was rinsed in de-ionized water and blown with nitrogen gas.

The transparent conducting oxide (TCO) film or window layer was ZnO(Al) which was deposited on the CdS/CIGS/Mo/SLG by RF-magnetron sputtering from the ceramic target (ZnO + 2.5 wt% Al_2O_3). The TCO film was a bi-layer film. The bottom layer was a highly resistive (≈ 50 nm thick) layer

prepared by reactive sputtering using Ar + 4 at% O_2, whereas the top layer was a highly conductive (≈ 500 nm thick) layer by the sputtering using only Ar gas.

The top metallic grids or front electrodes (total thickness ≈ 1.5 μm) of the solar cell devices were fork-shape Al(Ni) films which were deposited by thermal evaporation through a metallic mask. Each metallic grid was designed to give an individual cell with the total area of 0.48 cm^2, having 2.5% shading loss. The whole sample of 5x6 cm^2 can be scribed into 40 cells with 8 rows x 5 columns (not included the edged cells) as shown in Fig. 4.3.

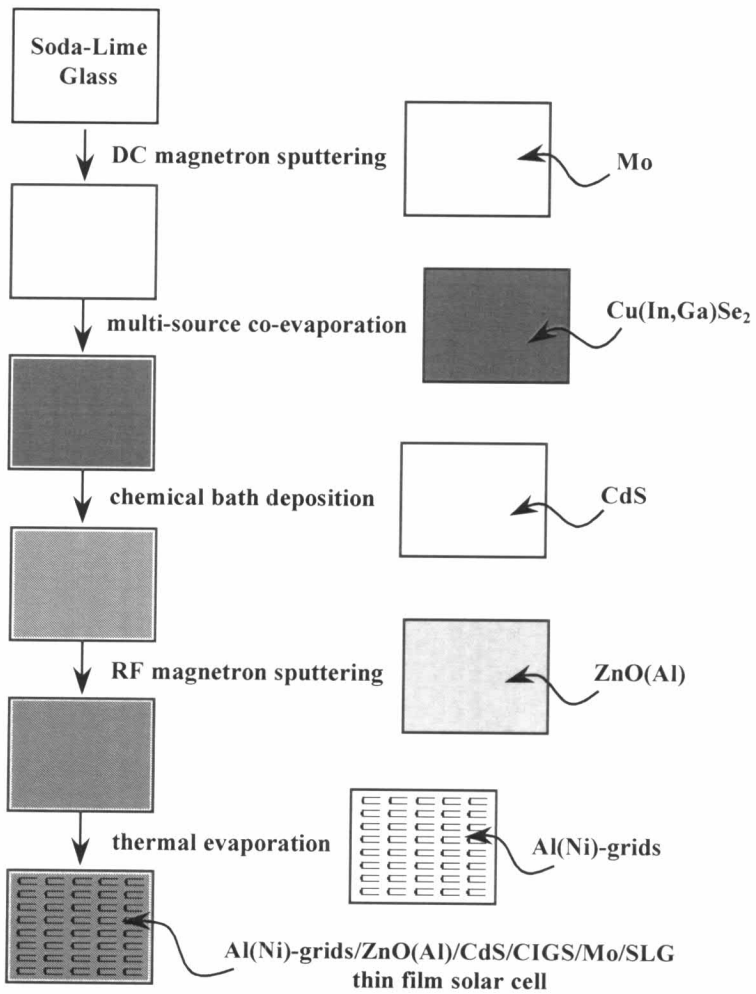

Figure 4.2: Schematic diagram of the CIGS fabrication process.

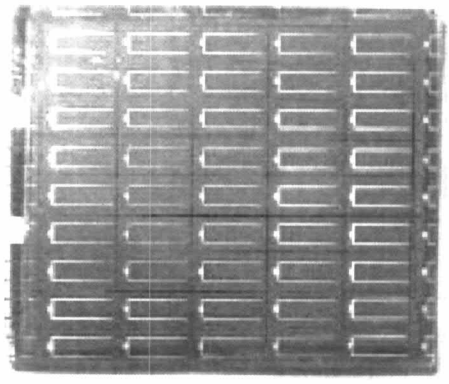

Figure 4.3: Photograph of the CIGS thin film solar cells (8 rows x 5 columns) fabricated at SPRL.

4.2 Growth of CIGS Thin Films by PVD Technique

4.2.1 General Calculation for CIGS Deposition Process

For $CuIn_{1-x}Ga_xSe_2$ films, the chemical composition is commonly defined by the atomic ratios y = [Cu]/([In]+[Ga]) and x = [Ga]/([In]+[Ga]). The [Cu]/([In]+[Ga]) ratio largely affects the film morphology while the [Ga]/([In]+[Ga]) ratio determines the band gap of the absorber layer. These parameters (x and y) are also used to characterize the composition of $Cu(In,Ga)Se_2$ material. During the growth process, these parameters as a function of time can be expressed as:

$$y = \frac{N_{Cu}}{N_{In} + N_{Ga}} \quad , \qquad (4.1)$$

and

$$x = \frac{N_{Ga}}{N_{In} + N_{Ga}} \quad . \qquad (4.2)$$

Here N_i is the number of atoms of specie i accumulated in the growing film at time t.

Consider both y and x in a unit area of CIGS film with a total thickness of d_{CIGS}. From Eqs. (4.1) and (4.2) the more general form of the atomic ratios can be written as:

$$y = \frac{d_{Cu} \cdot \rho_{Cu} \cdot M_{Cu}^{-1} \cdot A \cdot N_A}{(d_{In} \cdot \rho_{In} \cdot M_{In}^{-1} + d_{Ga} \cdot \rho_{Ga} \cdot M_{Ga}^{-1}) \cdot A \cdot N_A} \quad , \qquad (4.3)$$

and $$x = \frac{d_{Ga} \cdot \rho_{Ga} \cdot M_{Ga}^{-1} \cdot A \cdot N_A}{(d_{In} \cdot \rho_{In} \cdot M_{In}^{-1} + d_{Ga} \cdot \rho_{Ga} \cdot M_{Ga}^{-1}) \cdot A \cdot N_A} \quad , \qquad (4.4)$$

where d_i is the film thickness of metal i at time t,

ρ_i is the density of the metal i,

M_i is the mass per mole of the metal i,

A is the unit area of the growing film,

and N_A is Avogadro's constant.

The numerical values of the parameters are given in Table 4.1.

Table 4.1: Density and mass per mole values of the materials.

Material	ρ (g/cm^3)	M (g/mole)
Cu	8.96	63.55
In	7.31	114.82
Ga	5.91	69.72
Se	4.79	78.96
CIS	5.89	336.29
CGS	5.27	291.19

To simplify the expressions of y and x in Eqs. (4.3) and (4.4) respectively, we will define the parameter α_i as the following:

$$\alpha_{Cu} = \rho_{Cu} \cdot M_{Cu}^{-1} \quad , \qquad (4.5a)$$

$$\alpha_{In} = \rho_{In} \cdot M_{In}^{-1} \quad , \qquad (4.5b)$$

and $$\alpha_{Ga} = \rho_{Ga} \cdot M_{Ga}^{-1} \quad , \qquad (4.5c)$$

where the numerical values are given in Table 4.2.

Table 4.2: α parameter of the elements.

Material	$\alpha \equiv \rho/M$ (mole/cm^3)
Cu	0.1410
In	0.0637
Ga	0.0848
Se	0.0607

Substitute Eqs (4.5a), (4.5b) and (4.5c) back into Eqs. (4.3) and (4.4), we will get the relations of the corresponding metal film thicknesses,

$$d_{In} \cdot \alpha_{In} + d_{Ga} \cdot \alpha_{Ga} = d_{Cu} \cdot \alpha_{Cu} \cdot \frac{1}{y} = d_{Ga} \cdot \alpha_{Ga} \cdot \frac{1}{x}. \qquad (4.6)$$

Rearrange Eq. (4.6), we obtain

$$d_{Ga} = \frac{x}{y} \cdot \frac{\alpha_{Cu}}{\alpha_{Ga}} \cdot d_{Cu} \quad , \qquad (4.7a)$$

and $$d_{In} = \frac{(1-x)}{y} \cdot \frac{\alpha_{Cu}}{\alpha_{In}} \cdot d_{Cu} \quad . \qquad (4.7b)$$

According to the fact that at constant source temperature, the thickness d_i is proportional to the deposition rate of element i; r_i, and the deposition time t_i. Thus

$$d_i = r_i \cdot t_i \quad , \qquad (4.8)$$

Then, Eqs (4.7a) and (4.7b) can be rewritten as

$$r_{Ga} = \frac{x}{y} \cdot \frac{\alpha_{Cu}}{\alpha_{Ga}} \cdot r_{Cu} \quad , \qquad (4.9a)$$

and $$r_{In} = \frac{(1-x)}{y} \cdot \frac{\alpha_{Cu}}{\alpha_{In}} \cdot r_{Cu} \quad . \qquad (4.9b)$$

Eqs. (4.7a) and (4.7b) show the relation between the thickness of In and Ga films and the final composition and the thickness of Cu film. For example: stoichiometric CIS i.e. x=0, y=1, we obtain $d_{In} = 2.214\, d_{Cu}$, and for stoichiometric CGS i.e. x=1, y=1, we obtain $d_{Ga} = 1.663\, d_{Cu}$.

The relation between the thickness of the CIGS layer and the thickness of the corresponding Cu film made from the Cu contents of the CIGS can be calculated as

$$\frac{d_{Cu}}{d_{CIGS}} = \frac{V_{Cu}}{V_{CIGS}} = \frac{N_{Cu} \cdot M_{Cu} / \rho_{Cu}}{N_{CIGS} \cdot M_{CIGS} / \rho_{CIGS}} \quad , \qquad (4.10)$$

where V_{Cu} is the volume of copper layer,

V_{CIGS} is the volume of CIGS layer,

N_{Cu} is the number of copper atoms in the volume V_{Cu},

and N_{CIGS} is the number of CIGS molecules in the volume V_{CIGS}.

Due to the fact that $Cu(In_{1-x}Ga_x)Se_2$ (CIGS) layer is an alloy of two compounds, $CuInSe_2$ (CIS; x=0) and $CuGaSe_2$ (CGS; x=1). Hence, M and ρ are functions of x, then Eq. (4.10) can be written as

$$\frac{d_{Cu}}{d_{CIGS}} = \frac{N_{Cu} \cdot (M_{Cu}) \cdot (\rho_{CIS} \cdot (1-x) + \rho_{CGS} \cdot x)}{N_{CIGS} \cdot (M_{Cu} + M_{In} \cdot (1-x) + M_{Ga} \cdot x + 2 \cdot M_{Se}) \cdot (\rho_{Cu})} . \quad (4.11)$$

The ratio of N_{Cu} and N_{CIGS} is equal to unity. For example: CIS i.e. $x = 0$, we obtain: $d_{Cu} = 0.124\, d_{CIGS}$, and for CGS i.e. x=1, we obtain: $d_{Cu} = 0.128\, d_{CIGS}$.

4.2.2 The Two-Stage or Cu-Rich-Off (CURO) Process

The temperature profiles of sources and substrate of CIGS film deposited by CURO process is shown in Fig. 4.4.

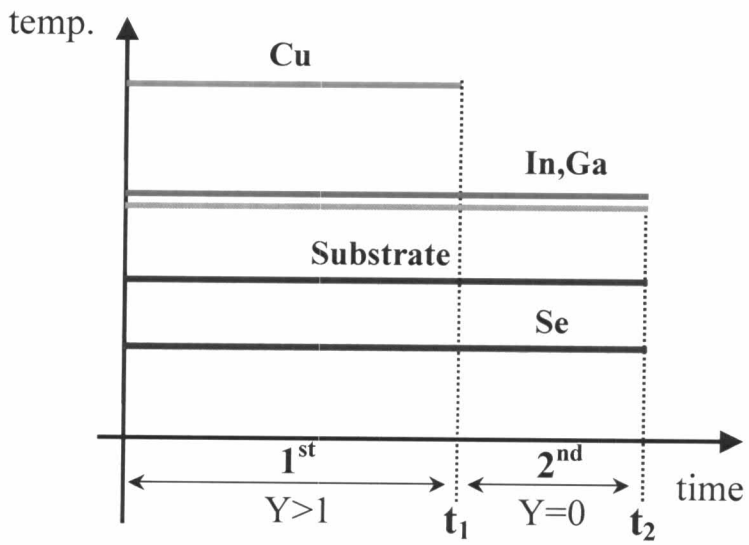

Figure 4.4: Temperature profiles of sources and substrate for CIGS film deposition by CURO process, Y being a ratio of Cu flux; $\Phi_{Cu}/(\Phi_{In}+\Phi_{Ga})$.

Consider the two following features of the Fig. 4.4, (i) source temperatures are constant, (ii) all of the Cu is deposited prior to t_1. Thus, the thickness of Cu, d_{Cu}, can be written as

$$d_{Cu}(t_1) = d_{Cu}(t_2) \quad . \qquad (4.12)$$

Substitute Eqs. (4.8) and (4.9a) into Eq. (4.12), we obtain

$$\frac{y(t_1)}{x} \cdot \frac{\alpha_{Ga}}{\alpha_{Cu}} \cdot r_{Ga}(t_1) \cdot t_1 = \frac{y(t_2)}{x} \cdot \frac{\alpha_{Ga}}{\alpha_{Cu}} \cdot r_{Ga}(t_2) \cdot t_2 . \qquad (4.13)$$

Since all sources temperature are constant, so the deposition rate of Ga (r_{Ga}) is constant during the deposition process; $r_{Ga}(t_1) = r_{Ga}(t_2)$, thus Eq. (4.13) can be written as

$$y(t) = \frac{y(t_1)}{t} \cdot t_1 \quad \text{for } t \geq t_1 \quad , \qquad (4.14)$$

where $y(t_1) \cdot t_1 = y(t_2) \cdot t_2$.

From Eq. (4.14), the evolution of the compositions of film, $y(t)$ and $x(t)$ is shown in Fig. 4.5.

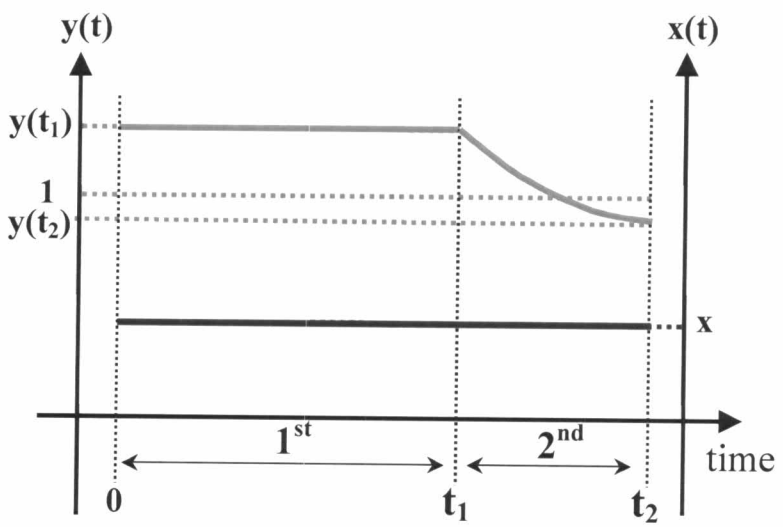

Figure 4.5: Evolution of film compositions, $y(t)$ and $x(t)$ during the deposition process of temperature profiles in Fig. 4.4.

Figure 4.4 and 4.5 show that the process starts with the deposition of Cu-rich film (y >1; with Cu-rich flux (Y>1; Y = $\Phi_{Cu}/(\Phi_{In}+\Phi_{Ga})$) in the first stage while all source temperatures are kept constant. At the end of the first stage ($t = t_1$), the Cu source is turned off (Y=0). In the second stage, the Cu-content, y, of the growing film decreases from Cu-rich to Cu-poor (see Fig. 4.5). We have named the two-stage process described above as CURO (**Cu-R**ich-**O**ff). At the end of the deposition process ($t = t_2$), the final desired composition, $y(t_2)$, can be obtained by *in situ* monitoring. During the deposition process, the Ga-content, x, of the growing film is kept constant. The temperatures of substrate (T_{sub}) and selenium (T_{Se}) are chosen at some values, depending on film quality and compositional requirements (e.g. T_{sub} is controlled at 500°C and T_{Se} at 250 °C).

The use of the theory described above can be shown by an example. We start by imposing the total film thickness (d_{CIGS}), the total process time (t_2) and the final film composition (x and $y(t_2)$). Then the thickness of the copper film (d_{Cu}) can be determined from Eq. (4.11). In order to set a Cu-rich condition in the 1st stage, one of two parameters; Cu time (t_1), or Cu-rich ($y(t_1)$) must be chosen to fit in Eq. (4.14). The deposition rate of Cu (r_{Cu}) can be calculated by Eq. (4.8) and can be converted to source temperature (T_{Cu}) as discussed in Section 3.2.5. The other parameters for In and Ga sources can also be calculated by using Eqs. (4.9a) and (4.9b), respectively.

For example, if the required data for the deposition process are given in Table 4.3, then the calculated values for the temperature profiles can be determined and shown in Table 4.4.

Table 4.3: Required data for the deposition process.

Required data	
d_{CIGS}	2.0 μm
t_1	1800 s
t_2	3000 s
$y(t_2)$	0.90
x	0.30

Table 4.4: Calculated values using the required data in Table 4.3.

Calculated values	
d_{Cu}	2507 Å
r_{Cu}	1.393 Å/s
T_{Cu}	1059 °C
$y(t_1)$	1.50
r_{Ga}	0.463 Å/s
T_{Ga}	660 °C
r_{In}	1.439 Å/s
T_{In}	763 °C

4.2.3 The Modified Two-Stage or Cu-Poor-Rich-Off (CUPRO) Process

In this research, we have modified the two-stage process (as shown in Fig. 4.6) in which the initial growth within the time t_{1a} is Cu-poor condition with constant r_{Cu}. After t_{1a} the r_{Cu} is increased and film become Cu-rich. At $t=t_1$ the Cu source is turned off. Therefore, the Cu-ratio, y, of the growing film decreases from Cu-rich to Cu-poor (see Fig. 4.7). We also have named the

modified two-stage process CUPRO in reference to the evolution of the Cu flux (**Cu**-**P**oor-**R**ich-**O**ff).

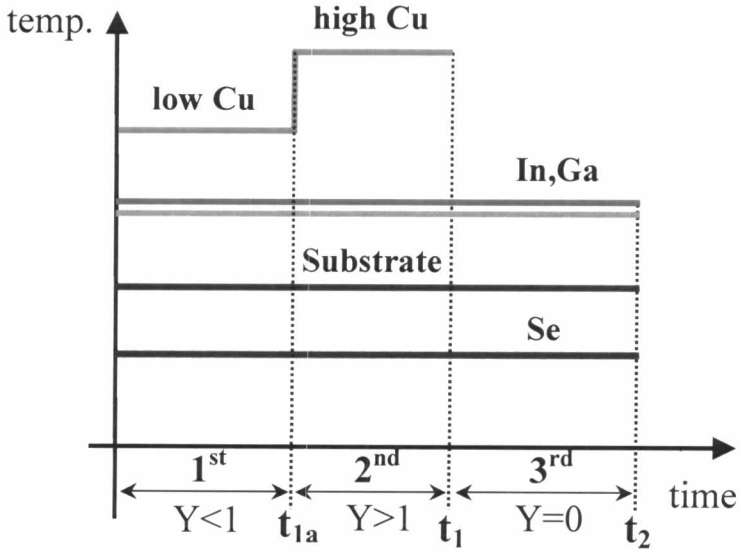

Figure 4.6: Temperature profiles of sources and substrate for CIGS film deposition by CUPRO. Y being a ratio of Cu flux.

The Cu-content in the CUPRO deposition process can be calculated similar to that previously described. In CUPRO deposition process, the relation between t_{1a}, t_1 and t_2 can be written as

$$d_{Cu}(t_{1a}) + d_{Cu}(t_1 - t_{1a}) = d_{Cu}(t_1) = d_{Cu}(t_2) \quad . \qquad (4.15)$$

Substitute Eqs. (4.8) and (4.9a) into Eq. (4.15), we obtain

$$y(t_{1a}) \cdot t_{1a} + y(t_1 - t_{1a}) \cdot (t_1 - t_{1a}) = y(t_1) \cdot t_1 = y(t_2) \cdot t_2 \quad . \qquad (4.16)$$

Thus, the important expression between Cu-content and deposition time in the CUPRO process can be written as

$$y(t) = \frac{y(t_{1a}) \cdot t_{1a} + y(t_1 - t_{1a}) \cdot (t - t_{1a})}{t} \quad \text{for } t_{1a} \le t \le t_1,$$

$$= \frac{y(t_1)}{t} \cdot t_1 \quad \text{for } t \ge t_1 \qquad , \qquad (4.17)$$

where $y(t_1 - t_{1a}) = \frac{y(t_1) \cdot t_1 - y(t_{1a}) \cdot t_{1a}}{(t_1 - t_{1a})}$.

From Eq. (4.17) and Fig. 4.6, the evolution of film composition *y(t)* and *x(t)* is shown in Fig. 4.7.

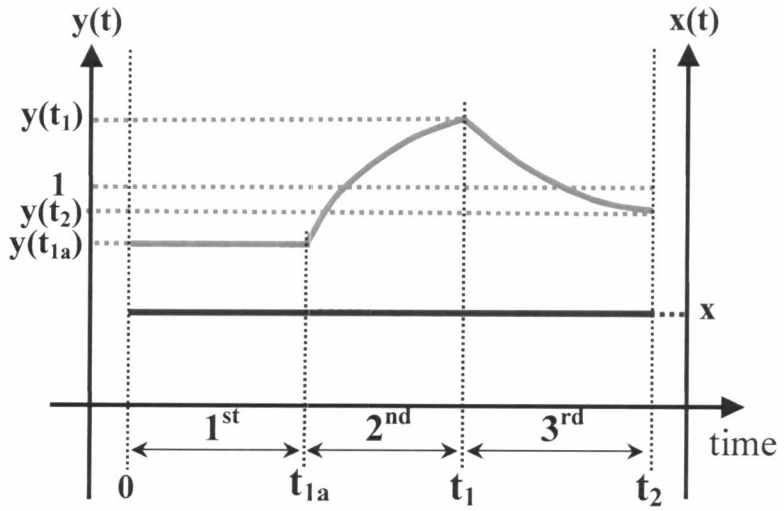

Figure 4.7: Evolution of film compositions, y(t) and x(t), of the temperature profiles in Fig. 4.6.

In principle, the method of calculating a set of temperature profiles for the CUPRO process is similar to that for the CURO process.

4.3 Characterization of CIGS Thin Films

In this research, morphology and composition of CIGS films were characterized from the same CIGS films by TEM and SEM equipped with EDS and their crystal structures by X-ray diffraction (XRD). The SEM micrographs were carried out from several systems (e.g. JEOL 6700F and LEO 1550). The TEM micrographs were carried out from a Joel 2000 FXII operating at 200kV and the XRD patterns were carried out from several systems (e.g. Bruker D8 advance and Siemens D5000).

In general, SEM requires a conducting sample in a high vacuum chamber but for non-conducting samples a very thin gold film is applied to reduce charging effects. SEMs often have a microprobe for energy dispersive analysis by studying the characteristic X-ray lines for rapid evaluation of elemental constituents.

The characteristic X-ray emitted from CIGS thin film when bombarded by focused electron beams on a small area of sample surface can be measured in EDS mode in SEM. The EDS is performed for acceleration voltages of 20 kV. A typical X-ray spectrum from EDS measurement of a CIGS thin film is shown in Fig. 4.8.

The distributions of X-ray intensities at the peaks of Cu, In, Ga and Se can be determined by the peak-fitting method. This method is able to figure and identify the characteristic X-rays of the elements in the sample and also can deduce the atomic weight percent of Cu, In, Ga and Se of CIGS sample. Hence, the atomic compositions of CIGS thin film can be determined.

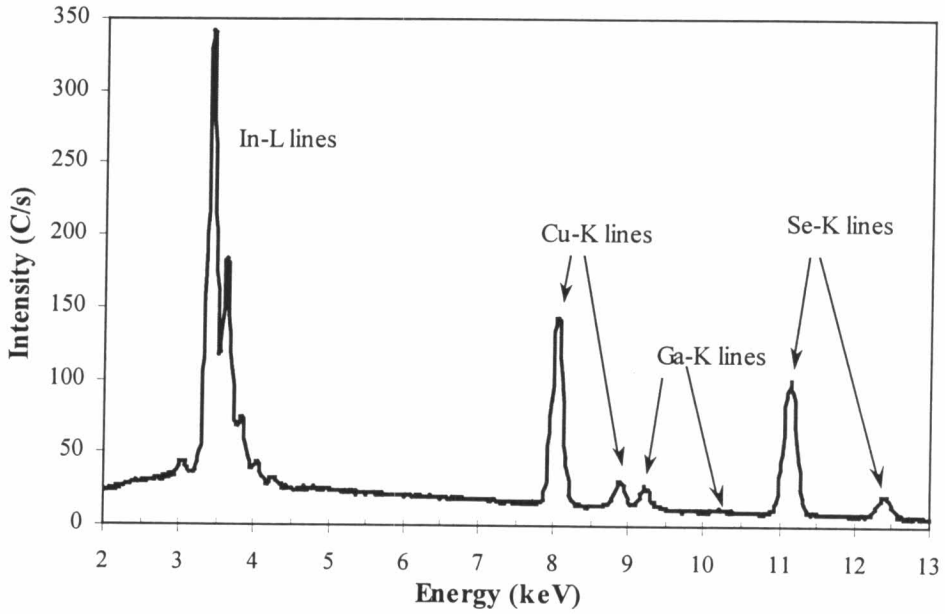

Figure 4.8: X-ray spectrum of a CIGS thin film

The peaks of Cu-K lines, In-L lines, Ga-K lines and Se-K lines in the X-ray spectrum were chosen and fitted by using the Gaussian function (G);

$$G = I \times exp\left[-0.5 \times \left(\frac{E-C}{W}\right)^2\right] \quad , \qquad (4.18)$$

and

$$W = \frac{FWHM}{2 \times \sqrt{2 ln 2}} . \quad , \qquad (4.19)$$

where I is the amplitude of the peak,

E is the energy,

C is the energy at the center of the peak,

W is the width of peak calculated using Eq. (4.19),

and $FWHM$ is the full width at half maximum of the peak.

Then by integrate Eq. (4.18), we obtain the peak area

$$A = \int_{-\infty}^{+\infty} I \times exp\left[-0.5 \times \frac{(E-C)^2}{W^2} \right] dE \quad , \qquad (4.20)$$

$$A = I \times W \times \sqrt{2\pi} \quad . \qquad (4.21)$$

The background intensity of the spectrum was fitted using quadratic function of X-ray energy. Then, it was subtracted from the spectrum giving only the characteristic X-rays of each element in the spectrum. After that, the characteristic X-rays of each peak were fitted to a Gaussian function by using Eq. (4.18). Finally, the peak area can be obtained by Eq. (4.21).

The peak area of this CIGS standard sample will be used as standard for normalized peak area of typical X-ray spectrum of CIGS thin films. The normalize peak area of each peak can be calculated for the atomic weight percent of Cu, In, Ga and Se including the ratios of [Cu]/([In]+[Ga]) and [Ga]/([In]+[Ga]).

4.4 Characterization of Cell Performance

In parallel to the CIGS film analysis, solar cells were produced from the same CIGS films where all other layers were fabricated using the baseline recipes in each laboratory. The cell performance were characterized using the standard measurements of current-voltage (I-V) and quantum efficiency (QE).

4.4.1 Current-Voltage (I-V) Measurement

The cell performances were measured under standard test condition (AM1.5, T=25°C) using a typical solar simulator based on a single 300W-ELH lamp (tungsten-halogen light source), normalized to a light intensity of 100 mW/cm^2 as illustrated in Fig. 4.9. The cell sample was placed on a temperature controlled stage (25±2°C) and contacted with two-point probe configuration. A Keithley model 238 was used as current source and voltage measurement. These signals were real-time accessed to display on a PC via IEEE-488 interface card and the parameters of cell characteristics (e.g. series resistance R_s, shunt resistance R_{sh}, open-circuit voltage V_{oc}, short-circuit current J_{sc}, fill factor FF and efficiency η) can be determined.

(a)

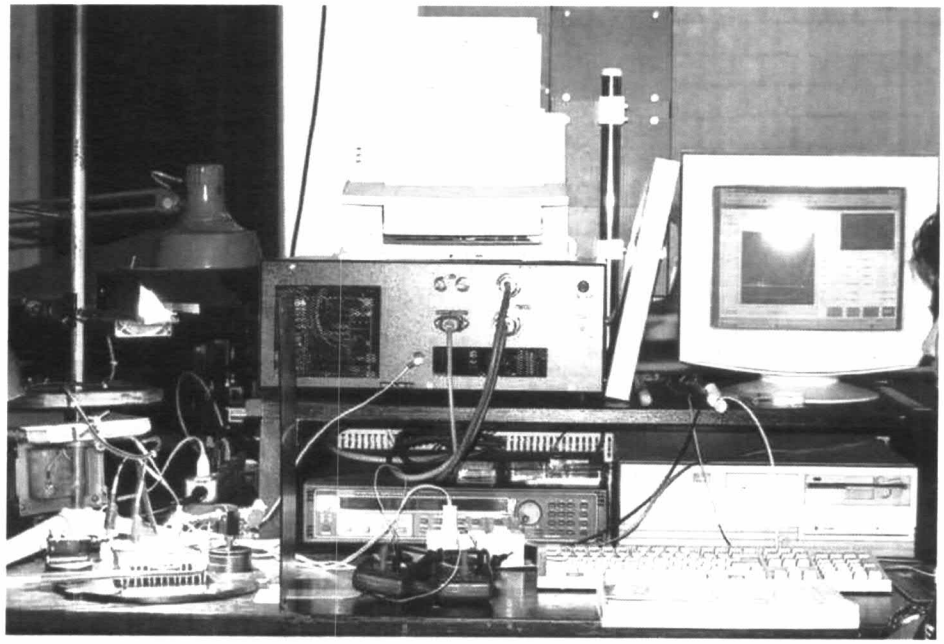

(b)

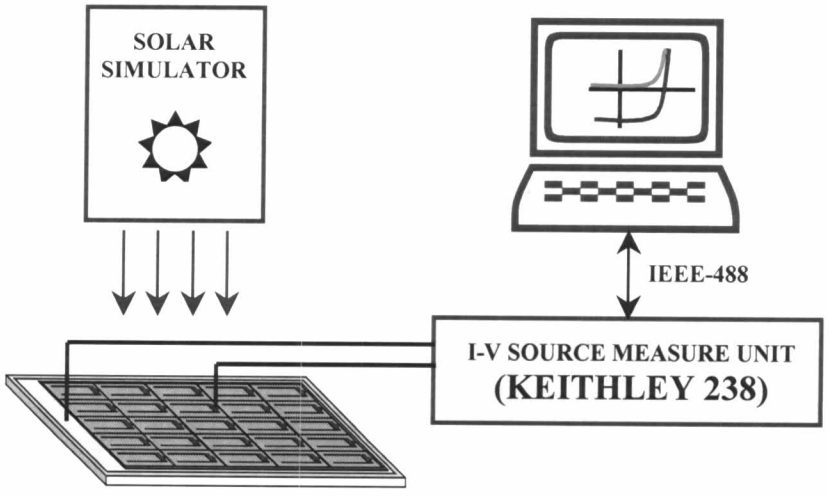

Figure 4.9: (a) Photograph of the I-V measurement system, (b) Schematic diagram of the I-V measurement system.

4.4.2 Quantum Efficiency (QE) Measurement

The quantum efficiency, QE, is the ratio of the number of carriers collected by the solar cell to the number of photons at a given wavelength of the incident light. On the other hand, QE is a measurement of how efficiently a device can convert incoming photons to charge carriers in an external circuit. QE is measured using the experimental set-up shown in Fig. 4.10.

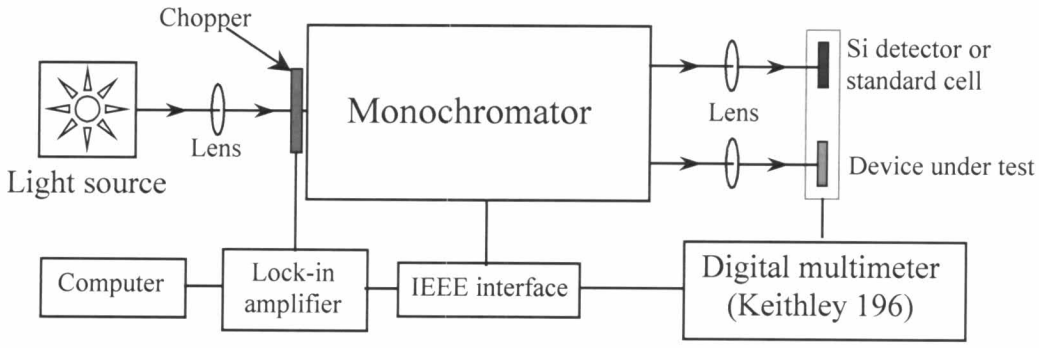

Figure 4.10: Schematic diagram of QE measurement set-up.

The quantum efficiency set-up used in the research has a Tungsten-halogen lamp as a light source. A monochromator provides a monochromatic light with a wavelength range from 400 to 1200 nm. The monochromator has adjustable entrance and exit slits. A matched pair of biconvex lenses are mounted on an optical rail to focus the light onto the sample or a silicon photodetector. The sample is mounted on a specially constructed holder that ensures incident light impinging perpendicularly. The device current (I_{device}) produced from the monochromatic light is measured and converted to an ac voltage signal across a 100 kΩ resistor. A lock-in amplifier locks into the

chopper frequency of the light signal and measures the corresponding ac voltage produced by the light.

A large area silicon detector with calibrated quantum efficiency, $QE_{detector}(\lambda)$, was used to find the device quantum efficiency. Once the detector photocurrent, $I_{detector}(\lambda)$, is measured and the device quantum efficiency, $QE_{device}(\lambda)$ can be determined using Eq. (4.22),

$$QE_{device}(\lambda) = \frac{I_{device}(\lambda) \times QE_{detector}(\lambda)}{I_{detector}(\lambda)} \quad . \qquad (4.22)$$

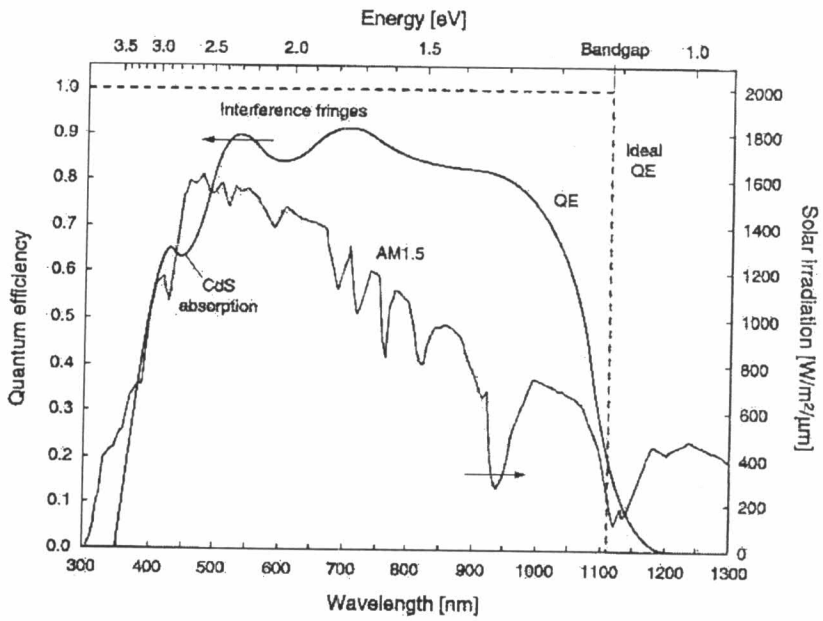

Figure 4.11: Typical wavelength resolved quantum efficiency plot of a CIGS solar cell, the solar spectrum (AM1.5) also shown in the figure [48].

Figure 4.11 shows a typical quantum efficiency plot of a CIGS solar cell (solid line). The measurement was taken over wavelengths from 400 to 1200 nm. This is the external quantum efficiency, i.e. it includes the effects of optical

losses such as transmission and reflection. Ideally, the quantum efficiency is a square (dotted line shown in Fig. 4.11), but in reality it is reduced due to recombination effects. The dip in the curve at around 450 nm is characteristic for CIGS solar cells and is caused by absorption in the thin CdS buffer layer. In addition, the curve often includes a number of interference fringes as indicated. A measure of the "true" short-circuit current density of the device under test is obtained by integrating the quantum efficiency multiplied with the solar spectrum.